Electrolytic Reduction of Spent Nuclear Oxide Fuel as Part of an Integral Process to Separate and Recover Actinides from Fission Products

S. D. Herrmann[a]; S. X. Li[a]; M. F. Simpson[a]; S. Phongikaroon[a]

[a] Fuel Cycle Programs Division, Idaho National Laboratory, Idaho Falls, Idaho, USA

PLEASE SCROLL DOWN FOR ARTICLE

Taylor & Francis
Taylor & Francis Group

Electrolytic Reduction of Spent Nuclear Oxide Fuel as Part of an Integral Process to Separate and Recover Actinides from Fission Products

S. D. Herrmann, S. X. Li, M. F. Simpson, and S. Phongikaroon

Fuel Cycle Programs Division, Idaho National Laboratory,
Idaho Falls, Idaho, USA

Abstract: Bench-scale tests were performed to study an electrolytic reduction process that converts metal oxides in spent nuclear fuel to metal. Crushed spent oxide fuel was loaded into a permeable stainless steel basket and submerged in a molten salt electrolyte of LiCl–1 wt% Li_2O at 650°C. An electrical current was passed through the fuel basket and a submerged platinum wire, effecting the reduction of metal oxides in the fuel and the formation of oxygen gas on the platinum wire surface. Salt and fuel samples were analyzed, and the extent of fission product separation and metal oxide reduction was determined.

Keywords: Electrolytic reduction, oxide reduction, pyrochemical processing, electrometallurgical treatment, spent oxide fuel treatment, molten $LiCl/Li_2O$

INTRODUCTION

An electrometallurgical treatment (EMT) process is operating at the Idaho National Laboratory (INL) for the separation and recovery of actinides from fission products in spent nuclear fuel. The EMT process is operated per the U.S. Department of Energy's (DOE's) Advanced Fuel Cycle Initiative

(AFCI) for the treatment of spent fuel from Experimental Breeder Reactor II (EBR-II). Engineering-scale treatment of spent EBR-II fuel, a sodium-bonded uranium metal alloy fuel in stainless steel cladding, has been ongoing since 1996 in hot cells at the INL Materials and Fuels Complex (formerly Argonne National Laboratory–West). The EMT process involves the anodic dissolution of the chopped, clad, metal fuel in a molten salt electrolyte (i.e., LiCl/KCl/UCl$_3$) and the simultaneous deposition of actinides on select cathode materials. The cathode deposits are removed from the electrolyte and further processed to remove adhering salt, yielding refined actinide materials that are separated from fission products and cladding. During the dissolution process the fission products partition into either the salt phase or remain in an undissolved metal phase (including the cladding hulls), each of which is subsequently processed into ceramic and metal waste forms, respectively (1).

To extend the capability of actinide separation and recovery from the EMT process to oxide fuels, a head-end step is necessary to convert (reduce) an oxide fuel to metal. Development of a particular reduction process (electrolytic reduction) that is compatible with the prescribed EMT process was initiated by Argonne National Laboratory and demonstrated at bench-scale with unirradiated oxide fuels (2). Demonstration of the electrolytic reduction process at bench scale was performed with *spent* oxide fuel at the INL Materials and Fuels Complex, which is the subject of this article.

In the electrolytic reduction process, spent oxide fuel is crushed and loaded into a permeable steel basket, which is submerged in a molten salt electrolyte of LiCl–1 wt% Li$_2$O at 650°C. A power supply is connected to the fuel basket (the cathode) and to a submerged platinum wire (the anode). A controlled electric current is passed between the cathode and anode to effect the reduction of oxide fuel to metal and the formation of oxygen gas on the platinum wire surface. The reduced metal remains in the submerged cathode basket and the oxygen gas is allowed to surface and dissipate from the electrochemical cell. The overall cell reaction is

$$M_xO_y \longrightarrow xM + y/2\,O_2(g),$$
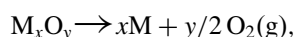
where M is the fuel constituent metal.

Two series of electrolytic reduction experiments (total of 10 runs) were conducted with spent oxide fuel (from a light water reactor) using an electrochemical apparatus inside of an argon atmosphere hot cell. The purpose of the bench-scale experiments was to demonstrate and characterize the electrolytic reduction process with spent oxide fuel. Specifically, the partitioning of fission products between the salt and fuel phases was determined. Also, the extent of metal oxide reduction in the fuel basket was quantified.

EXPERIMENTAL

Apparatus

The electrolytic reduction experiments were performed in an existing bench-scale electrochemical cell called the Hot Fuel Dissolution Apparatus (HFDA). The HFDA was located in the main cell of the INL Hot Fuel Examination Facility (HFEF)−an argon atmosphere hot cell. Crucibles and probes specific to the electrolytic reduction experiments were fabricated and configured in the heated zone of the HFDA as shown in Fig. 1.

The fabricated and installed components to the experimental apparatus included a steel liner that contained a 10-cm diameter by 11-cm tall magnesia oxide crucible, and a set of stainless steel heat shields that were ported for 5 contacting probes−one center port and 4 outer ports that were 90 degrees apart on a 3.5-cm radius. The center port was configured with a thermocouple assembly that was electrically isolated from the HFDA. Three of the outer ports were configured with a cathode fuel basket, an anode, and a reference electrode. The remaining unoccupied port was used for periodic salt sampling.

The fuel baskets were fabricated from a 3-ply layer of perforated stainless steel sheet metal (outer surface), 325-mesh stainless steel wire cloth (middle layer), and 18-mesh stainless steel wire cloth (inner layer), all of which were diffusion bonded together by a commercial supplier (Purolator). The permeable baskets were formed into closed-end cylinders of 1.9-cm diameter by 5.7-cm tall. The top open end of the basket cylinder was welded to an armature that suspended an electrically isolated stainless steel
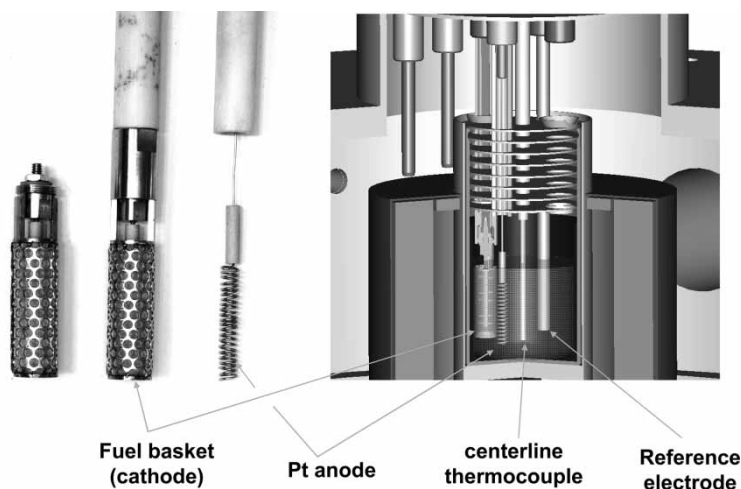

Fuel basket (cathode)   **Pt anode**   **centerline thermocouple**   **Reference electrode**

Figure 1. Fabricated equipment for electrolytic reduction of spent oxide fuel in Hot Fuel Dissolution Apparatus (Sectional View).

center lead. The fuel basket was fitted to electrically isolated extension rods that connected the basket wall and center lead to separate power supplies outside of the HFDA containment. The prescribed fuel basket was used for the first 9 of 10 experiments, and a modified basket was used for the final experiment. The final basket was modified by replacing the perforated sheet metal and mesh composite with a 1.9-cm diameter by 5-cm tall stainless steel sintered metal basket, as shown in Fig. 2.

The anode was fabricated from 1-mm diameter platinum wire (99.95%, Johnson Matthey) that was wound to form a 0.6-cm diameter by 5-cm tall helix. A 0.6-cm diameter by 2.5-cm tall section of magnesia tube was located concentric to and on top of the spiral-wound platinum wire. Approximately 50-cm of platinum wire was in contact with the molten salt electrolyte during the experiments. The upper end of the platinum wire was fixed above the salt level to an electrically isolated extension rod, which was connected to a power supply outside of the HFDA containment.

A reference electrode was fabricated from a high density, closed-end magnesia tube with a porous end plug (Ozark Technical Ceramics). The tube was filled with 900 mg of nickel (II) oxide (99.998%, Puratronic) and fitted with a nickel wire (99.98%, Alfa Aesar). The electrically isolated nickel wire extended outside of the HFDA containment and was connected to a potentiostat and Data Acquisition System (DAS). The reference
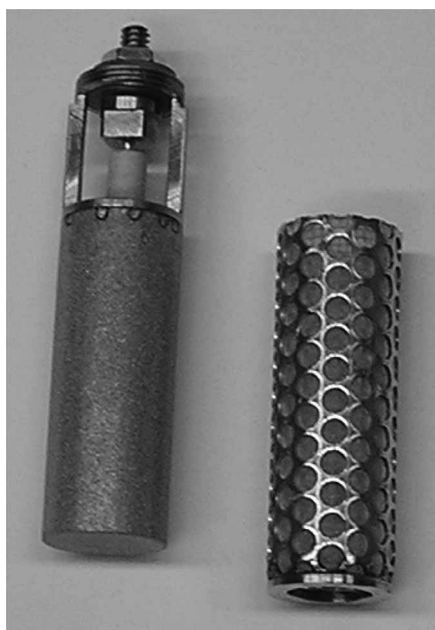

Figure 2. Sintered metal fuel basket assembly for final run (left) and perforated sheet metal and 325 mesh fuel basket (right).

electrode provided a Ni/NiO coupling with the molten salt electrolyte to monitor relative anode and cathode potentials.

The HFDA was electrically configured as shown in Fig. 3. Power supplies, potentiostats, and data acquisition systems for the HFDA were located outside of the hot cell. Cyclic voltammetry was performed with an EG&G Princeton Applied Research model 273A potentiostat/galvanostat (first series of experiments) and a Solartron model 1285 potentiostat (second series of experiments). Data were monitored and recorded with a Hewlett Packard Model 349070A Data Acquisition/Switch Unit. The primary and secondary currents were supplied by separate KEPCO Bipolar Operational Power Supplies/Amplifiers.

Spent Nuclear Oxide Fuel

The electrolytic reduction experiments were conducted with spent light water reactor fuel from Belgium Reactor 3 (BR3). One entire element of fuel that was irradiated in BR3 in 1979 was used in the reduction experiments. The element consisted of a 1-m tall UO_2 fuel column in a 9.5-mm diameter Zircaloy-4 cladding. The fuel was initially enriched in U-235 at 8.3 wt%, was irradiated to a mean specific burn-up of 35.7 GWd/t, and had decayed for 26 years at the time of the subject experiments. The fuel element was sectioned, and the fuel was crushed and sieved into 5 particle size ranges: (1) below 0.045 mm, (2) 0.045 to 0.6 mm, (3) 0.6 to 1.2 mm, (4) 1.2 to 2.8 mm, and (5) 2.8 to 4 mm. A portion of the first particle size range was sampled and subjected to chemical and radiochemical analysis; the results are shown in Table 1.
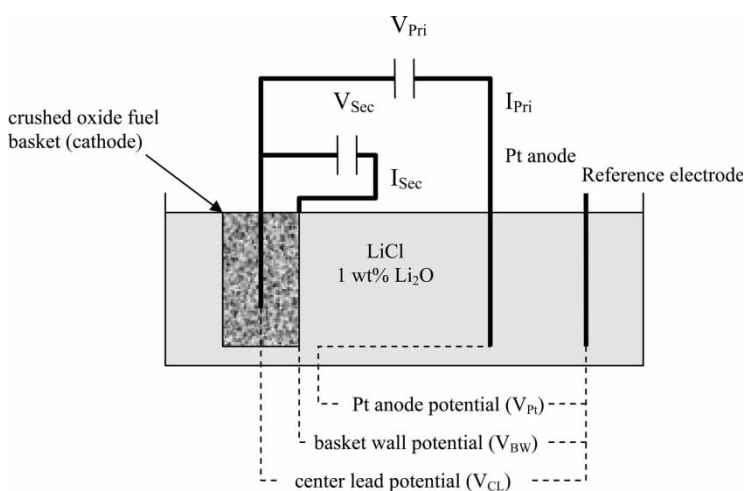

Figure 3. Schematic of electrolytic reduction cell.

Table 1. Constituent concentrations in irradiated BR3 oxide fuel

Rare earths (ppm)		U/TRU (ppm)		Noble metals (ppm)		Salt soluble (ppm)	
Nd	4200	U-total	838000	Zr	3300	Cs	2500
Ce	2600	Pu-total	6060	Mo	2600	Ba	2200
La	1300	Np-237	421	Ru	1200	Sr	790
Pr	1200	Am-241	230	Tc	540	Rb	530
Sm	830			Pd	470	Te	490
Y	560			Rh	280	Eu	100

Procedure

Ten electrolytic reduction runs were performed in 2 separate series of experiments involving 3 crucible loadings of molten salt electrolyte, as outlined in Table 2. The first 3 runs were performed successively in the same electrolyte solution (crucible A), allowing salt-soluble fission products to accumulate in the electrolyte. The electrolyte solution was replaced with clean salt (crucible B) for the fourth run. After completing analysis of salt and fuel samples from the first series of tests (runs 1 through 4), a new electrolyte solution (crucible C) was prepared and a second series of runs was conducted. All 6 runs in the second series of experiments were performed in succession in the same electrolyte, allowing fission products to accumulate in the salt.

Preparation of the 3 new crucible loadings that were placed in service before runs 1, 4, and 5 included insertion of a centerline thermocouple and reference electrode, both of which remained in the salt for the duration of their respective succession of experiments. Cyclic Voltammetry (CV) was performed with each electrolyte solution prior to conducting electrolytic

Table 2. Test matrix for electrolytic reduction experiments

Series	Cruible	Run	Particle size (mm)	Fuel mass (g)
I	A	1	1.2–2.8	46.71
		2	1.2–2.8	46.01
		3	1.2–2.8	41.00
	B	4	0.045–0.6	50.30
II	C	5	0.045–0.6	45.81
		6	2.8–4.0	45.40
		7	2.8–4.0	40.86
		8	0.6–1.2	52.57
		9	0.6–1.2	56.37
		10	<0.045	28.44

reduction runs in order to characterize the cell and identify anode and cathode reaction potentials relative to the reference electrode. Indeed, the potential values used throughout this article are relative to the Ni/NiO reference electrode, unless otherwise stated.

An electrolytic reduction run was performed by filling a fuel basket with a prescribed quantity of crushed BR3 oxide fuel, as shown in Table 2. The basket was then attached to its extension rods, lowered into the molten salt, and connected to the primary and secondary power supplies. The spiral wound platinum anode was lowered into the salt, connected to the primary power supply and energized. The primary current (I_{pri}) was controlled to maintain the basket center lead potential (V_{CL}) below lithium formation potential and the platinum anode potential (V_{Pt}) below that which would cause the platinum to dissolve, as predetermined by CV. The secondary current (I_{sec}) was initiated once the potential on the basket wall (V_{BW}) indicated the presence of lithium metal.

At the conclusion of an electrolytic reduction run, the platinum anode and fuel basket were removed from the HFDA. The same platinum anode was used in runs 1 through 4 and another for runs 5 through 10. Select fuel baskets were sectioned and sampled (runs 1 through 4 and 7), and the balance were placed in sealed storage containers for subsequent electrorefining tests, which will further examine the separation and recovery of actinides from fission products by the previously described electrometallurgical techniques for metal fuels. Salt samples were extracted before and after each electrolytic reduction run. Some of the salt samples were collected and subjected to extensive chemical and radiochemical analysis in a separate analytical laboratory hot cell following each series of tests. Others were analyzed the same day in an adjacent HFEF hot cell for lithium oxide concentration, allowing maintenance of the electrolyte at approximately 1 wt% Li_2O.

Analysis of the fuel samples required a separation of the metal and oxide phases. This was accomplished by dissolving a fuel sample with elemental bromine in an ethyl acetate medium. The bromine dissolved the metals in the fuel sample, leaving the oxide compounds in the solid phase. The solid phase was separated from the ethyl acetate solution by multiple centrifuging, decanting, and washing evolutions. The separated solid phase was dissolved in acid in preparation for constituent analyses. The technique to separate the metal and oxide phases of the fuel samples was developed by Argonne National Laboratory, based on previous work by others (3, 4). The prescribed technique was validated in the hot cell analytical laboratory for the separation of U and UO_2. The technique should apply to transuranic, noble metal, and rare earth fission products. However, without validation of each specific constituent metal and oxide combination, the results for the transuranic, noble metal, and rare earth constituents can only be considered preliminary.

Inductively Coupled Plasma–Mass Spectroscopy (ICP-MS) was used to analyze total U (U-234, U-235, U-236, U-238), total Pu (Pu-238, Pu-239, Pu-240, Pu-241, Pu-242), Np-237, and Am-241 in all of the fuel and salt

samples and I-127, I-129, and Tc-99 in salt and fuel samples for runs 5–10. Inductively Coupled Plasma–Optical Emission Spectroscopy (ICP-OES) was used to analyze all other listed constituents, except cesium, in the salt and fuel samples. Total cesium was analyzed by atomic absorption in runs 1 through 4, and by ICP-MS (Cs-133 and Cs-135) and gamma spectroscopy (Cs-137) in runs 5 through 10.

RESULTS AND DISCUSSION

The standard potentials ($E°$) for the major constituent reactions in the electrolytic reduction process at 650°C are shown below (5).
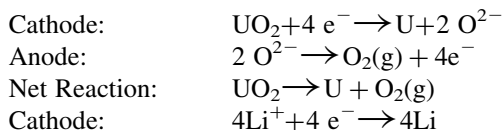
$$UO_2 \longrightarrow U + O_2 \qquad E° = 2.40\,V$$
$$Li_2O \longrightarrow 2Li + 1/2O_2 \qquad E° = 2.47\,V$$
$$LiCl \longrightarrow Li + 1/2Cl_2 \qquad E° = 3.46\,V$$
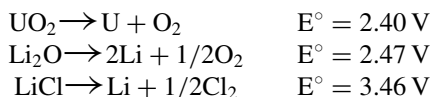
The standard potentials of UO_2 and Li_2O differ by approximately 70 mV. Even though the prescribed salt system (LiCl -1 wt% Li_2O) is not at standard conditions, the potential difference between UO_2 and Li_2O is sufficiently small to make operation of the cell difficult for UO_2 reduction alone. Consequently, the electrolytic reduction experiments with spent oxide fuel were conducted such that both uranium and lithium reduction occurred at the cathode. An advantage in lithium metal generation at the location of uranium oxide is it will chemically reduce the oxide fuel as follows (5),

$$4Li + UO_2 \longrightarrow U + 2Li_2O \qquad \Delta G(650°C) = -27\,kJ/mol$$

where ΔG is the Gibbs free energy.

A disadvantage in lithium metal generation is its capability of diffusing through the salt and attacking the platinum anode. To mitigate the attack of lithium on the platinum anode, the electrolytic reduction cell was configured with an additional power supply as shown in Fig. 3. The current from the primary power supply was controlled to effect the reduction of uranium oxide and lithium oxide while preventing the anodic dissolution of platinum. The current from the secondary power supply was controlled to mitigate the diffusion of lithium metal outside the cathode basket by oxidizing the lithium metal (to Li^+) upon contact with the basket wall. Thus, the major half-cell and net reactions that occurred in this system for the primary and secondary power supplies are listed below.

Primary Power Supply:

Cathode:	$UO_2 + 4\,e^- \longrightarrow U + 2\,O^{2-}$
Anode:	$2\,O^{2-} \longrightarrow O_2(g) + 4e^-$
Net Reaction:	$UO_2 \longrightarrow U + O_2(g)$
Cathode:	$4Li^+ + 4\,e^- \longrightarrow 4Li$

Anode: $2\,O^{2-} \longrightarrow O_2(g) + 4\,e^-$
Net Reaction: $4\,Li^+ + 2\,O^{2-} \longrightarrow 4\,Li + O_2\,(g)$

Secondary Power Supply:

Cathode: $Li^+ + e^- \longrightarrow Li$
Anode: $Li \longrightarrow Li^+ + e^-$
Net Reaction: Li/Li^+ cycle
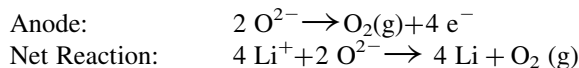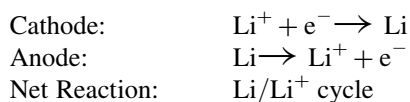
The first solution of molten salt was prepared by loading 700 g of LiCl (99.99%, less than 100 ppm moisture, Aldrich-APL) into a magnesia crucible and heating it in the HFDA to 650°C. A total of 7 g of Li_2O (99.6%, Alfa Aesar) was added to the LiCl in 4 equal increments. CV was performed before and after each Li_2O addition. The CV runs utilized separate stainless steel and platinum wires (1-mm diameter) as working electrodes, and a spiral-wound 2-mm diameter carbon steel wire as a counter electrode. The carbon steel counter electrode was immersed in the salt to a depth of approximately 5 cm and provided a surface area that was more than 100 times larger than either the stainless steel or platinum working electrodes. The counter electrode remained in the salt throughout the series of CV runs. The stainless steel and platinum working electrodes were introduced into the salt alternately for each of the Li_2O concentrations (0, 0.25, 0.5, 0.75, and 1.0 wt%). After immersing each working electrode in the salt (to a depth of approximately 1 cm), a potentiostat was used to apply a potential to the working electrode at a specified scan rate (nominally 25 mV/sec) that began at an open circuit potential and lowered (stainless steel working electrode) or rose (platinum working electrode) to a set vertex potential and then returned to the open circuit potential. The cyclic voltammagrams for the stainless steel and platinum working electrodes are shown in Figs. 4 and 5, respectively.   CV with the stainless steel working electrode (Fig. 4) identified the cathode potential at which lithium metal was generated for the varying concentrations of Li_2O. For the nominal Li_2O concentration of 1 wt% in the electrolyte, the onset of lithium formation occurred at approximately -1.75 V. A notable shift in the lithium formation potential was observed between the voltammagrams for 0.25 and 0.5 wt% Li_2O concentrations. A similar shift in reaction potential was observed with platinum as the working electrode. Specifically, the platinum dissolution potential, as shown in Fig. 5, shifted from approximately $+1.4$ V at 0.25 wt% Li_2O to $+1.65$ V at 0.5 wt% Li_2O. The cyclic voltammagrams at 0.75 and 1 wt% Li_2O did not reach platinum dissolution due to the current limitation (1 A) of the potentiostat. Consequently, $+1.65$ V was used as the upper limit for the anode potential in subsequent reduction runs to avoid platinum dissolution. The voltammagram at 1 wt% Li_2O for the platinum working electrode identified an anode potential of approximately $+0.85$ V at which oxygen ions began to oxidize to oxygen gas.
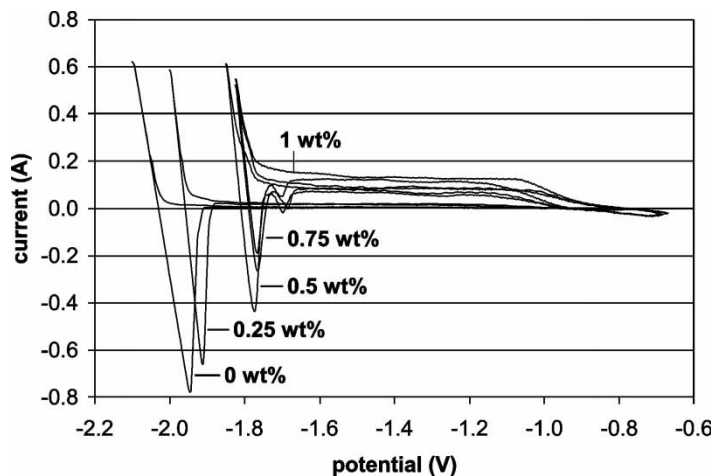
Figure 4. Cyclic voltammetry with stainless steel working electrode for varying Li_2O concentrations.

CV was performed for each of the 3 new crucible loadings and similar results were obtained, including the shift in reaction potentials at working electrodes between 0.25 and 0.5 wt% Li_2O. CV was also performed on the electrolytic reduction baskets after they were loaded with spent oxide fuel and immersed in the electrode. Cyclic voltammagrams from reduction basket no.5 with 1 wt% Li_2O in the electrolyte are shown in Fig. 6 and
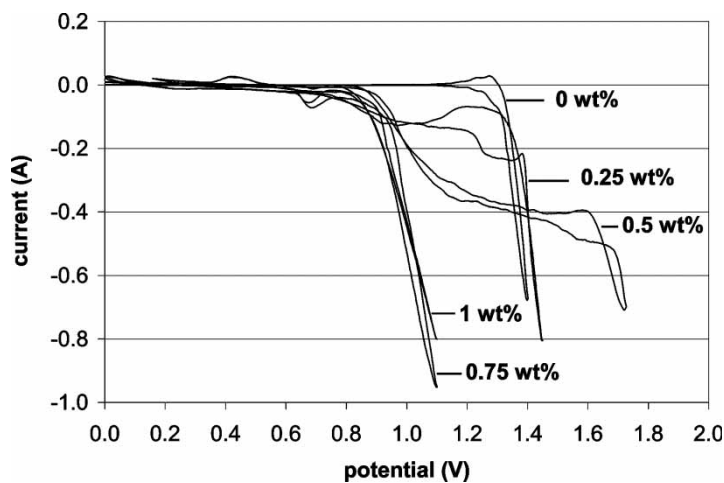
Figure 5. Cyclic voltammetry with platinum working electrode for varying Li_2O concentrations.
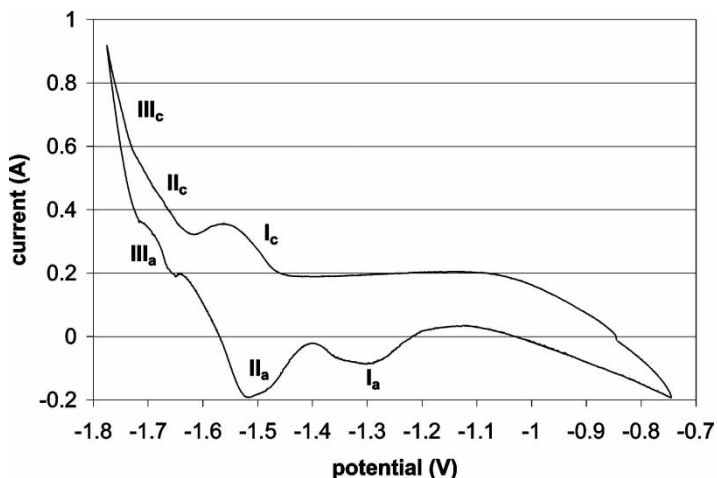
Figure 6. Cyclic voltammetry with BR3 fuel in stainless steel basket as working electrode for LiCl–1 wt% Li_2O.

again in Fig. 7 (superimposed with the voltammagram for a bare stainless steel working electrode at 1 wt% Li_2O). The cyclic voltammagrams for the fifth reduction basket distinguish the reactions zones for UO_2 reduction versus lithium reduction. Furthermore, the plots appear to distinguish between the suspected reactions within the system, i.e., $U^{4+} \leftrightarrow U^{3+}$ (cathodic peak I_c and anodic return peak I_a in Fig. 6), $U^{3+} \leftrightarrow U^{\circ}$ (peaks II_c and II_a), and $Li^+ \leftrightarrow Li$ (peaks III_c and III_a).

Figure 7. Cyclic voltammetry with BR3 fuel in stainless steel basket and stainless steel wire (no fuel) as working electrodes for LiCl–1 wt% Li_2O.

Following each CV test with spent fuel, the leads from the electrolytic reduction basket were switched from a potentiostat to controlled current power supplies. The spiral-wound platinum anode was immersed into the electrolyte, and the primary power supply was energized. The primary and secondary currents and the potentials of the platinum, basket wall, and basket center leads were monitored throughout each run. These m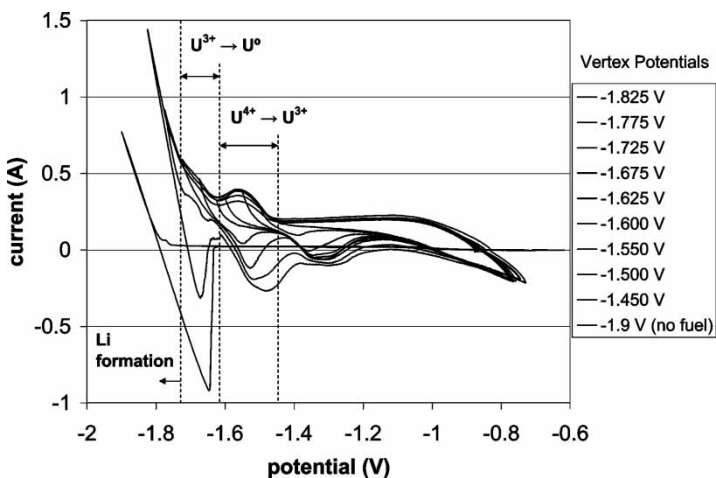easured data are shown in Fig. 8 as a function of Faraday charge for run 5. Figure 8 illustrates how the primary current was gradually raised to and maintained at 3 A, except for two overnight periods when the primary and secondary currents were relaxed to less than 100 mA to preclude significant reactions while the system was unattended. After approximately 220% of the theoretical charge had been passed, the anode potential began to rise rapidly, indicating a completion of the UO_2 reduction and a consequent lowering of oxygen ion activity in the electrolyte from continued Li_2O decomposition. This phenomenon continued to be observed while stepping down the primary and secondary currents until both power supplies were de-energized after passing 47.4 A-hr of integrated current (Faraday charge of 2.61 in Figure 8). The cathode baskets following each electrolytic reduction run were removed and select fuel baskets were sectioned, as shown in Fig. 9, revealing a metallic sheen on the cut surfaces of the packed fuel bed. Those select fuel baskets that were sectioned (runs 1 through 4 and 7) were also sampled, and the balance were placed in sealed storage containers for subsequent electrorefining tests.

The final run was performed with the < 0.045-mm fuel fines. In order to retain the fuel fines, the fuel basket was modified as described previously (see Fig. 2). There were notable differences in performance between the final run and previous runs. The fuel loading (28.44 g) was lower for the final run, and the achievable current was restricted to 1 A to prevent the platinum anode
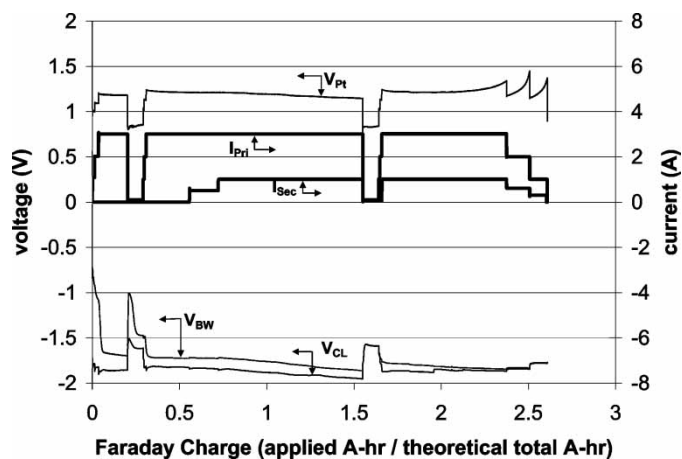

Figure 8.   Response plot from electrolytic reduction run 5 with BR3 spent oxide fuel.

Figure 9. Post-test fuel section of the first electrolytic reduction run with BR3 spent oxide fuel.

from dissolving. In addition, the applied charge necessary to achieve complete reduction in the final run was significantly higher than previous runs, resulting in an approximate cell efficiency of 21% as opposed to 33 to 45% for other runs.

Samples of the salt were withdrawn before and after each reduction run and subjected to chemical and radiochemical analyses. The post-test salt sample for a given run also served as the pre-test salt sample for the following run in a series. Samples of post-test fuel from runs 1 through 4 and 7 were likewise subjected to analysis. The analytical results for the salt and fuel samples are shown in Table 3a and Table 3b for test series I and II, respectively. The salt sample results identify the constituent concentrations (ppm) in the salt, while the select fuel sample results identify the constituents in fractions (wt%) between the metal and oxide phases. The results of the fuel samples for runs 2 and 3 are not presented due to the questionable storage conditions of the samples (i.e., the caps to the sample containers were found loose after the containers had stood for a prolonged period of time in an air atmosphere prior to analysis).

The distribution of fuel constituents between the salt and fuel phases behaved largely as expected. The salt soluble fission products cesium, barium, strontium, and iodine clearly diffused into and accumulated in the salt phase. Rubidium, tellurium, and europium were also expected to separate from the fuel and accumulate in the salt phase; however, their concentrations were largely below the detections limits for the applied ICP-OES analytical technique. Tellurium and europium, however, were detected in the salt following run 4. Although run 4 commenced with a new salt

Table 3a. Pre-and post-test salt and fuel analysis for test series I

Crucible	A						B			
Run	1				2	3	4			
Phase	Salt, pre-run	Fuel, metal	Fuel, oxide	Salt, post-run	Salt, post-run	Salt, post-run	Salt, pre-run	Fuel, metal	Fuel, oxide	Salt, post-run
Conc.	ppm	wt%	wt%	ppm	ppm	ppm	ppm	wt%	wt%	ppm
Salt-soluble fission products										
Cs	ND			129–150	190–231	308–354	ND			111–119
Ba	ND			85–140	210–220	310–330	40			140
Sr	ND			40–60	85–90	130–140	15			65
Rb	ND			ND	ND	ND	ND			ND
Te	ND			ND	ND	ND	ND			75
Eu	ND			ND	ND	ND	ND			15
Uranium/Transuranics										
U-total	6	98	2	5–11	10–15	3–9	50–82	98–99	1–2	2–5
Pu-total	2	87	13	0.4–4	0.6–0.8	0.4–1.3	1.9	93–96	4–7	0.3–0.4

Np-237	ND	98	2	ND	ND	ND	0.3	97–98	2–3	0.3–0.6
Am-241	ND	68	32	ND	ND	ND	ND	77–84	16–23	ND
Rare earths										
Nd	ND	8	92	ND	ND	ND	ND	36–43	57–64	ND
Ce	ND	ND	> 81	ND	ND	ND	ND	40–49	51–60	ND
La	ND	ND	> 89	ND	ND	ND	ND	ND	ND	ND
Pr	ND	ND	> 89	ND	ND	ND	ND	38–47	53–62	ND
Sm	ND	ND	> 67	ND	ND	ND	ND	27–33	67–73	ND
Y	ND	ND	> 90	ND	ND	ND	ND	34–40	60–66	ND
Noble metals										
Zr	ND	ND	ND	ND	ND	ND	ND	ND–45	55– > 94	ND
Mo	ND	94	6	ND	ND	ND	ND	90–92	8–10	ND
Ru	ND	> 90	ND	ND	ND	ND	ND	84–87	13–16	ND
Tc	ND	> 94	ND	ND	ND	ND	ND	> 88	ND	ND
Pd	ND	ND	ND	ND	ND	ND	ND	> 75	ND	ND
Rh	ND	> 75	ND	ND	ND	ND	ND	64–71	29–36	ND

Notes: ND = non-detectable (below minimum detection levels).

S. D. Herrmann et al.

Table 3b. Pre-and post-test salt and fuel analysis for test series II

Crucible	C								
Run	5		6	7			8	9	10
Phase	Salt, pre-run	Salt, post-run	Salt, post-run	Fuel, metal	Fuel, oxide	Salt, post-run	Salt, post-run	Salt, post-run	Salt, post-run
Conc.	ppm	ppm	ppm	wt%	wt%	ppm	ppm	ppm	ppm
Salt-soluble fission products									
Cs	ND	125	200–215			295	435–440	590	690–710
Ba	ND	120	120–180			210	310–340	520–560	620–630
Sr	ND	60	65			90	130–140	210–230	250
Rb	ND	ND	ND			ND	ND	ND	ND
Te	ND	ND	ND			ND	ND	ND	ND
Eu	ND	ND	ND			ND	ND	ND	ND
I-127	ND	ND	ND			ND	ND	ND–1.5	1.9–2.6
I-129	ND	ND	5.5–6.0			5.8	5.5–6.0	10.0–11.6	12.7–16.4
Uranium/Transuranics									
U-total	112	18–20	76–103	99.7	0.3	25	13–17	12–39	10–12
Pu-total	2	1.2–1.3	7.6–9.6	97.8	2.2	0.6	0.9–11.9	1.2–1.6	2.3

Np-237	ND	ND	ND	> 98.8	ND	ND	ND	ND	ND
Am-241	ND	ND	ND	90.2	9.8	ND	ND	ND	ND
Rare earths									
Nd	ND	ND	ND	65	35	ND	ND	ND	ND
Ce	ND	ND	ND	80	20	ND	ND	ND	ND
La	ND	ND	ND	ND	ND	ND	ND	ND	ND
Pr	ND	ND	ND	> 28	ND	ND	ND	ND	ND
Sm	ND	ND	ND	> 33	ND	ND	ND	ND	ND
Y	ND	ND	ND	69	31	ND	ND	ND	ND
Noble metals									
Zr	ND	ND	ND	ND	ND	ND	ND	ND	ND
Mo	ND	ND	ND	> 97	ND	ND	ND	ND	ND
Ru	ND	ND	ND	> 83	ND	ND	ND	ND	ND
Tc-99				> 99.5	ND				
Pd	ND	ND	ND	> 50	ND	ND	ND	ND	ND
Rh	ND	ND	ND	> 76	ND	ND	ND	ND	ND

Notes: ND = non-detectable (below minimum detection levels).

loading and reference electrode, the same centerline thermocouple from runs 1 through 3 was used in run number 4. Consequently, some carryover of contaminated salt occurred, as evidenced by the presence of barium and strontium in the salt prior to run 4.

Since uranium and transuranic analyses in the salt phase were performed by ICP-MS, the detection limit was much lower for these constituents than the fission products. Consequently, uranium and plutonium were detected in the salt. However, there was no distinct trend in accumulation of these constituents. Also, the pre-test salt samples for runs 1, 4, and 5 should have been devoid of fuel and yet detectable levels of uranium, plutonium and even neptunium-237 (in the pre-test salt of run 4) were present. Thus, it was concluded that the minor presence of uranium and transuranic constituents in the salt phase was likely from sample contamination (due to component handling inside of a hot cell that routinely handles spent fuel), rather than from the diffusion and accumulation of BR3 fuel in the salt phase.

The reduction of metal oxides in the fuel basket occurred largely as expected, with the notable exception of zirconium. The analyses of fuel from runs 1, 4, and 7 showed a significant and comparable reduction of uranium, plutonium, and neptunium-237. The reduction of americium-241 was less significant, but still in excess of 68% for these runs. Some reduction of the rare earths was observed, notably in run 7, where roughly two thirds of the rare earth constituents were found in the metal phase. The noble metal constituents were predominantly found in the metal phase for fuel from runs 1, 4, and 7 with the exception of zirconium. Zirconium was not identified in either the metal or oxide phases of the fuel from run 1. Suspecting that the zirconium remained in the oxide phase, an additional step was applied to the analysis of fuel for run 4, which involved dissolution of the oxide phase with hydrofluoric acid to adequately dissolve any zirconium in the oxide phase. Zirconium was consequently detected in both the metal and oxide phases for the fuel from run 4. However, the zirconium was predominantly observed in the oxide phase (i.e., 55% to more than 94 wt% for run 4).

Cell efficiencies were calculated from the ratio of theoretical charge for the given fuel loading to the actual applied charge from primary current (i.e., the inverse of final Faraday charge). These reported cell efficiencies are considered approximate values since they include some reduction of lithium oxide in addition to uranium oxide. Cell efficiencies for runs 1, 4, and 5 through 9 ranged from 33 to 45% with no apparent dependency on particle size. However, there was a marked difference in cell efficiency (21%) for the final run, which is attributed to the use of a sintered metal versus 325 mesh containment of the fuel. The thickness and porosity of the sintered metal basket wall ($\sim$0.0625 in. thick, 20 micron porosity) versus that of the 325 mesh ($\sim$0.0011 in. thick, 45 micron nominal opening) would logically introduce a substantially larger barrier, through which the oxygen ions would have to diffuse to effect the electrolytic reduction process. This increased barrier was manifest by the significantly lower

attainable current (≤ 1 A) for the final run versus that (nominally 3 to 4 A) for all other runs.

CONCLUSION

Electrolytic reduction of irradiated oxide fuel was successfully performed at bench-scale in the HFEF. The distribution of fission products between the salt and fuel phases was quantified. Cesium, barium, strontium, and iodine diffused from the fuel and accumulated in the salt phase, as expected. The rare earth and noble metal fission products remained with the uranium and transuranic constituents in the reduced fuel basket. The extent of reduction of metal oxides in a fuel basket reached 99.7% for uranium, and comparable reduction efficiencies were observed for the transuranics, i.e., 97.8% for plutonium, $>98.8\%$ for neptunium, and 90.2% for americium. The rare earth and zirconium fission products were partially reduced and remained in the fuel basket. The noble metal fission products were predominantly found in the metal phase and likewise remained in the fuel basket. The impact of fission product accumulation on the electrolytic reduction process was inconclusive, due to an insufficient build-up of fission products in the electrolyte. The approximate cell efficiency for runs 1 and 4 through 9 ranged from 33 to 45%, while that for the final run achieved 21%, which is attributed to the difference in its fuel basket wall. The fuel from 5 of the latter runs was placed in sealed storage for subsequent electrorefining tests, which will further explore the separation and recovery of actinides from fission products.

REFERENCES

1. Benedict, R.W. and McFarlane, H.F. (1998) EBR-II spent fuel treatment demonstration project status. *RADWASTE*, 5 (4).
2. Gourishankar, K., Redey, L., and Williamson, M. (2002) Electrolytic reduction of metal oxides in molten salts, *Light Metals.*
3. Brunzie, G.F., Johnson, T.R., and Steunenberg, R.K. (1961) Selective dissolution of uranium from uranium—Uranium oxide mixtures by bromine-ethyl acetate. *Anal. Chem.*, 33: 1005–1006.
4. Ashbrook, A.W. (1962) The determination of uranium metal in products from the reduction of uranium oxides with magnesium. *Analyst*, 87: 751–754.
5. HSC Chemistry–Chemical reaction and equilibrium software with extensive thermochemical database. *Outokumpu Research.* **2002**, version 5.1.